

Manifold Density Estimation via Generalized Dequantization

James A. Brofos¹ Marcus A. Brubaker^{2,3} Roy R. Lederman¹

Abstract

Density estimation is an important technique for characterizing distributions given observations. Much existing research on density estimation has focused on cases wherein the data lies in a Euclidean space. However, some kinds of data are not well-modeled by supposing that their underlying geometry is Euclidean. Instead, it can be useful to model such data as lying on a *manifold* with some known structure. For instance, some kinds of data may be known to lie on the surface of a sphere. We study the problem of estimating densities on manifolds. We propose a method, inspired by the literature on “dequantization,” which we interpret through the lens of a coordinate transformation of an ambient Euclidean space and a smooth manifold of interest. Using methods from normalizing flows, we apply this method to the dequantization of smooth manifold structures in order to model densities on the sphere, tori, and the orthogonal group.

1. Introduction

Certain kinds of data are not well-modeled under the assumption of an underlying Euclidean geometry. Examples include data with a fundamental directional structure, data that represents transformations of Euclidean space (such as rotations and reflections), data that has periodicity constraints or data that represents hierarchical structures. In such cases, it is important to explicitly model the data as lying on a *manifold* with a suitable structure; for instance a sphere would be appropriate for directional data, the orthogonal group for rotations and reflections, and the torus captures structural properties of periodicity.

The contribution of this work is to express density estimation

¹Department of Statistics and Data Science, Yale University
²Department of Electrical Engineering and Computer Science, York University, Toronto, Canada
³Vector Institute, Toronto, Canada. Correspondence to: James A. Brofos <james.brofos@yale.edu>.

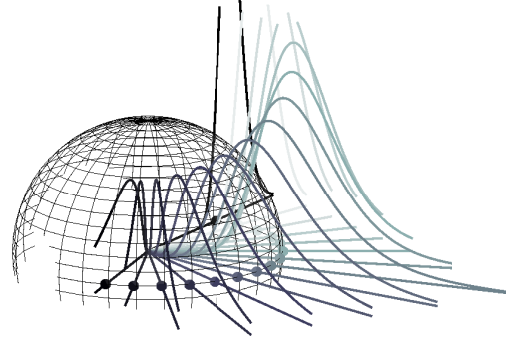


Figure 1. We model densities on a manifold as a projection, or “quantization,” onto the manifold from an ambient Euclidean space. To enable density computations we use a “dequantization density” which can depend position on the manifold. In this figure the manifold in question is \mathbb{S}^2 , embedded in \mathbb{R}^3 and the dequantization density, illustrated here for a set of locations along the equator of \mathbb{S}^2 , is over $r \in \mathbb{R}_+$, the distance from the origin in the direction $y \in \mathbb{S}^2$. Density on the manifold can be estimated via importance sampling by marginalizing over \mathbb{R}^+ for a given $y \in \mathbb{S}^2$ using the dequantization distribution as an importance distribution.

on manifolds as a form of dequantization. Given a probability density in an ambient Euclidean space, one can obtain the density on the manifold by performing a *manifold change-of-variables* in which the manifold structure appears and then projecting out any auxiliary structures. This marginalization can be viewed as analogous to “quantization” where, for instance, continuous values are discarded and only rounded integer values remain. In this view the auxiliary structure defines how the manifold could be “dequantized” into the ambient Euclidean space. By marginalizing along these auxiliary dimensions, one obtains the marginal distribution on the manifold. In practice, however, one has only the manifold-constrained observations from an unknown distribution on the manifold. A second contribution of this work is to formulate the density estimation as a learning problem on the ambient Euclidean space. We show how to invoke the manifold change-of-variables, and then perform the marginalization along the auxiliary dimensions to obtain effective estimates of the density on the manifold. An advantage of our dequantization approach is that it *allows one to utilize any expressive density directly on the ambient Euclidean space* (e.g., RealNVP (Dinh et al., 2017), neural

ODEs (Chen et al., 2018; Grathwohl et al., 2018) or any other normalizing flow (Kobyzev et al., 2020)); the dequantization approach does not require a practitioner to construct densities intrinsically on the manifold.

2. Illustrative Example: Sphere

We first offer a simple example to illustrate how the method may be applied to obtain densities on the sphere. Let $\mathbb{S}^2 \subset \mathbb{R}^3$ represent the 2-dimensional sphere viewed naturally as an embedded manifold of 3-dimensional Euclidean space. Excluding the point $(0, 0, 0) \in \mathbb{R}^3$, observe that every other point $x \in \mathbb{R}^3$ may be uniquely identified with a point $s \in \mathbb{S}^2$ and positive real number $r \in \mathbb{R}_+$ such that $x = rs$. Thus, $\mathbb{S}^2 \times \mathbb{R}_+$ represents a *spherical coordinate system* for $\mathbb{R}^3 \setminus \{0\}$. If $\pi_{\mathbb{R}^3}(x)$ is a density on \mathbb{R}^3 (equivalent to $\mathbb{R}^3 \setminus \{0\}$ up to a set of Lebesgue measure zero), we can apply the standard change-of-variables formula in order to obtain a density on $\mathbb{S}^2 \times \mathbb{R}_+$:

$$\pi_{\mathbb{S}^2 \times \mathbb{R}_+}(s, r) = r^2 \cdot \pi_{\mathbb{R}^3}(rs), \quad (1)$$

where r^2 is the associated Jacobian determinant accounting for changes in volume. We will refer to $\pi_{\mathbb{R}^3}$ as the *ambient Euclidean distribution*.

By sampling $x \in \mathbb{R}^3$ with density $\pi_{\mathbb{R}^3}(x)$, converting to the spherical coordinate system and discarding the radius r , we obtain a sample from the marginal distribution $\pi_{\mathbb{S}^2}$ on the sphere \mathbb{S}^2 . The density $\pi_{\mathbb{S}^2}$ is given by:

$$\pi_{\mathbb{S}^2}(s) = \int_{\mathbb{R}_+} \pi_{\mathbb{R}^3}(rs) r^2 dr = \int_{\mathbb{R}_+} \pi_{\mathbb{S}^2 \times \mathbb{R}_+}(s, r) dr \quad (2)$$

This density can be evaluated using importance sampling using a non-vanishing density $\tilde{\pi}_{\mathbb{R}_+}$ on \mathbb{R}_+ ,

$$\pi_{\mathbb{S}^2}(s) = \mathbb{E}_{r \sim \tilde{\pi}_{\mathbb{R}_+}} \frac{\pi_{\mathbb{S}^2 \times \mathbb{R}_+}(s, r)}{\tilde{\pi}_{\mathbb{R}_+}(r|s)}. \quad (3)$$

We note that $\tilde{\pi}_{\mathbb{R}_+}$ may depend on $s \in \mathbb{S}^2$. A visualization of these concepts is presented in fig. 1.

Equation (2) *quantizes* $\mathbb{S}^2 \times \mathbb{R}_+$ to \mathbb{S}^2 by integrating out the auxiliary dimension. Equation (3) describes how to marginalize $\pi_{\mathbb{S}^2 \times \mathbb{R}_+}$ over \mathbb{R}_+ to compute the density of a quantized point $s \in \mathbb{S}^2$; hence, we refer to $\tilde{\pi}_{\mathbb{R}_+}$ as the *dequantization density*. Taking the log of eq. (3), and invoking Jensen's inequality we can also obtain the following lower bound on the marginal log-probability of s :

$$\log \pi_{\mathbb{S}^2}(s) \geq \mathbb{E}_{r \sim \tilde{\pi}_{\mathbb{R}_+}} \log \frac{\pi_{\mathbb{S}^2 \times \mathbb{R}_+}(s, r)}{\tilde{\pi}_{\mathbb{R}_+}(r)}. \quad (4)$$

Finally, we can use eq. (1) to express both eq. (3) and eq. (4) in terms of the density on the ambient Euclidean space \mathbb{R}^3 .

2.1. Learning the Distributions: Sphere Example

In order to make these densities learnable, we introduce parameters $\theta \in \mathbb{R}^{n_{\text{amb}}}$ and $\phi \in \mathbb{R}^{n_{\text{deq}}}$ and write $\pi_{\mathbb{R}^3}(x) \equiv \pi_{\mathbb{R}^3}(x|\theta)$ and $\tilde{\pi}_{\mathbb{R}_+}(r) \equiv \tilde{\pi}_{\mathbb{R}_+}(r|\phi, s)$. For instance, $\pi_{\mathbb{R}^3}(x|\theta)$ could be a normalizing flow parameterized by θ and $\tilde{\pi}_{\mathbb{R}_+}(r|\phi, s)$ could be a log-normal distribution whose mean and variance parameters are determined by a neural network with parameters ϕ and input s .

We can use eq. (4) as an objective function for performing density estimation on the sphere. Given samples $\mathcal{D} = (s_1, \dots, s_{n_{\text{obs}}})$ we compute a lower bound on the marginal log-probability as,

$$\mathbb{E}_{s \sim \text{Unif}(\mathcal{D})} \log \pi_{\mathbb{S}^2}(s) \geq \mathbb{E}_{s \sim \text{Unif}(\mathcal{D})} \mathbb{E}_{r \sim \tilde{\pi}_{\mathbb{R}_+}} \log \frac{\pi_{\mathbb{R}^3}(rs|\theta)}{\tilde{\pi}_{\mathbb{R}_+}(r|s, \phi)/r^2}. \quad (5)$$

We can then maximize the right-hand side with respect to θ and ϕ . This yields a procedure for estimating the density on a sphere by transforming a density in an ambient Euclidean space and marginalizing over the radial dimension. The learned distribution on the ambient space $\pi_{\mathbb{R}^3}(x|\theta)$ is represented using a normalizing flow. This allows us to sample $x \sim \pi_{\mathbb{R}^3}(x|\theta)$ and to evaluate the density $\pi_{\mathbb{R}^3}(x|\theta)$. Therefore, to sample from the learned $\pi_{\mathbb{S}^2}$ we simply sample $x \sim \pi_{\mathbb{R}^3}(x|\theta)$, and then project it to the sphere: $s = x/\|x\|$.

2.2. Evaluating the Density: Sphere Example

Next, we may wish to evaluate the learned density $\pi_{\mathbb{S}^2}$. The normalizing flow provides us with the learned density $\pi_{\mathbb{R}^3}(x|\theta)$ in the ambient space, which immediately gives us the density $\pi_{\mathbb{S}^2 \times \mathbb{R}_+}$ through eq. (1), we must marginalize over \mathbb{R}_+ so as to obtain a density on \mathbb{S}^2 . We return to eq. (2) and use the dequantization distribution $\tilde{\pi}_{\mathbb{R}_+}$ to evaluate $\pi_{\mathbb{S}^2}(s)$ using importance sampling.

3. Related Work

The general problem of density estimation is well studied and a full review is beyond the scope of this paper. The most directly related work is in the area of density estimation with normalizing flows and we refer readers to the review articles by Papamakarios et al. (2019) and Kobyzev et al. (2020).

From the perspective of estimating general densities on smooth manifolds, our work is related to Rezende et al. (2020), which considers normalizing flows on tori and spheres. Bose et al. (2020) defines a class of normalizing flows on hyperbolic spaces. Wang & Gelfand (2013) considers the density of a multivariate normal random variable projected to the sphere via the mapping $x \mapsto x/\|x\|$. For methods on connected Lie groups, one may use the exponential map in order to smoothly parameterize an element of the group by a coordinate in Euclidean space; this was

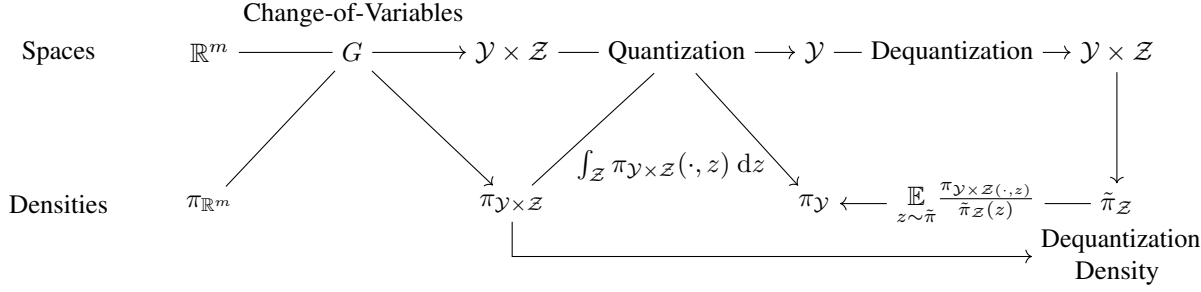


Figure 2. The dequantization roadmap. In the first row, we begin with \mathbb{R}^m (or a space identical to \mathbb{R}^m up to a set of measure zero). This Euclidean space can be transformed into the product of manifolds $\mathcal{Y} \times \mathcal{Z}$ via a change-of-variables $G : \mathbb{R}^m \rightarrow \mathcal{Y} \times \mathcal{Z}$. Quantization takes the product manifold $\mathcal{Y} \times \mathcal{Z}$ to its \mathcal{Y} -component alone. In the second row, we may begin with a probability density $\pi_{\mathbb{R}^m}$ defined on \mathbb{R}^m . Under the change-of-variables G we obtain a new probability density $\pi_{\mathcal{Y} \times \mathcal{Z}}$ which is related to $\pi_{\mathbb{R}^m}$ by the manifold change-of-variables eq. (8). Quantizing $\mathcal{Y} \times \mathcal{Z}$ marginalizes out the \mathcal{Z} -component of $\pi_{\mathcal{Y} \times \mathcal{Z}}$. We may equivalently introduce a dequantization density $\tilde{\pi}_{\mathcal{Z}}$ and compute the marginal density on \mathcal{Y} via importance sampling.

the approach adopted in Falorsi et al. (2019). Lou et al. (2020) extended continuous normalizing flows to manifolds by defining and simulating ordinary differential equations on the manifold. In contrast to these approaches, the method proposed here allows for the use of any density estimation technique defined on the ambient Euclidean space.

This work was inspired by dequantization techniques for normalizing flows. Originally introduced by Uria et al. (2013) to account for the discrete nature of pixel intensities, the basic approach added (uniform) continuous noise to discrete values. This prevented the pathological behaviour that is known to occur when fitting continuous density models to discrete data (Theis et al., 2016). The technique was extended by Ho et al. (2019) to allow the added noise distribution to be learned using a variational objective which has become critical for strong quantitative performance in image modelling. Hoogeboom et al. (2020) generalized the variational objective used for learning the dequantization noise distribution. Recently Lippe & Gavves (2021) extended normalizing flows to categorical distributions. Our work proposes a new perspective on these approaches that the ambient Euclidean space (over which a continuous density model is learned) is a product of a discrete space (e.g., pixel intensities or discrete categories) and a continuous space which is projected (or “quantized”) when data is observed. Our work is a generalization of dequantization to consider not only discrete spaces, but also other structured spaces, specifically non-Euclidean manifolds.

4. Preliminaries

Let Id_n denote the $n \times n$ identity matrix. If \mathcal{X} and \mathcal{Y} are isomorphic sets we denote this by $\mathcal{X} \cong \mathcal{Y}$. The set of \mathbb{R} -valued, full-rank $n \times p$ matrices ($n \geq p$) is denoted $\text{FR}(n, p)$. The set of full-rank $n \times n$ matrices is denoted $\text{GL}(n)$, the generalized linear group. A matrix $\mathbf{P} \in \mathbb{R}^{n \times n}$

is positive definite if for all $x \in \mathbb{R}^n$ we have $x^\top \mathbf{P} x > 0$. The set of all $n \times n$ positive definite matrices is denoted $\text{PD}(n)$. When $\mathbf{P} \in \text{PD}(n)$ is a positive-definite matrix we denote the principal matrix square root by $\sqrt{\mathbf{P}}$. We now consider several examples of embedded manifolds; see also appendix I for details on manifold embeddings.

Example 1 (Hypersphere). The sphere in \mathbb{R}^m is defined by, $\mathbb{S}^m = \{x \in \mathbb{R}^m : x^\top x = 1\}$. The sphere is an important manifold for data with a directional component (such as the line-of-sight of an optical receiver) or data that naturally lies on the surface of a spherical body (such as occurrences of solar flares on a star).

Example 2 (Torus). The torus is the product manifold of circles

$$\mathbb{T}^n \stackrel{\text{def.}}{=} \underbrace{\mathbb{S}^1 \times \cdots \times \mathbb{S}^1}_{n \text{ times}}. \quad (6)$$

The torus $\mathbb{T}^2 = \mathbb{S}^1 \times \mathbb{S}^1$ can be embedded in \mathbb{R}^4 by embedding each circle individually in \mathbb{R}^2 . The torus is an important manifold for studying systems with several angular degrees of freedom (such as applications to robotic arms) or systems with periodic boundaries (Rezende et al., 2020).

Example 3 (Stiefel Manifold and Orthogonal Group). The Stiefel manifold represents orthogonality constraints in a vector space. It may be regarded as the manifold of orthonormal vectors within a larger ambient Euclidean space. The Stiefel manifold can be leveraged for low-rank matrix completion. An important variant of the Stiefel manifold is the orthogonal group, which is the collection of all linear transformations of Euclidean space that preserve distance. The Stiefel manifold of order (n, p) is defined by,

$$\text{Stiefel}(n, p) \stackrel{\text{def.}}{=} \{\mathbf{M} \in \mathbb{R}^{n \times p} : \mathbf{M}^\top \mathbf{M} = \text{Id}_n\}. \quad (7)$$

The n^{th} orthogonal group is defined by $\text{O}(n) = \text{Stiefel}(n, n)$. Applications of the orthogonal group include

the Procrustes problem, which describes the optimal rotation and reflection transformations that best align one cloud of particles toward another (Doucet et al., 2001). The Stiefel manifold has found applications for low-rank matrix completion (Brubaker et al., 2012).

The *special* orthogonal group is a subgroup of $O(n)$ that satisfies the additional property that they have unit determinant. Formally, $SO(n) \stackrel{\text{def.}}{=} O(n) \cap \{\mathbf{M} \in \mathbb{R}^{n \times n} : \det(\mathbf{M}) = 1\}$.

5. Theory

For our theoretical development, the most important tool is the change-of-variables formula for embedded manifolds.

Theorem 1. Let \mathcal{Y} and \mathcal{Z} be smooth manifolds embedded in \mathbb{R}^n and \mathbb{R}^p , respectively. Let $G : \mathbb{R}^m \rightarrow \mathcal{Y} \times \mathcal{Z}$ be a smooth, invertible transformation. Let $\pi_{\mathbb{R}^m}$ be a density on \mathbb{R}^m . Under the change-of-variables G , the corresponding density on $\mathcal{Y} \times \mathcal{Z}$ is given by,

$$\pi_{\mathcal{Y} \times \mathcal{Z}}(y, z) = \frac{\pi_{\mathbb{R}^m}(x)}{\sqrt{\det(\nabla G(x)^\top \nabla G(x))}} \quad (8)$$

where $x = G^{-1}(y, z)$.

Even when G is not an invertible mapping, it may be possible to compute the change-of-variables when G is invertible on partitions of \mathbb{R}^m .

Corollary 1. Let $\mathcal{O}_1, \dots, \mathcal{O}_l$ be a partition of \mathbb{R}^m . Let $G : \mathbb{R}^m \rightarrow \mathcal{Y} \times \mathcal{Z}$ be a function and suppose that there exist smooth and invertible functions $G_i : \mathcal{O}_i \rightarrow \mathcal{Y} \times \mathcal{Z}$ such that $G_i = G|_{\mathcal{O}_i}$ for $i = 1, \dots, l$. Then, if $x \sim \pi_{\mathbb{R}^m}$, the density of $(y, z) = G(x)$ is given by

$$\pi_{\mathcal{Y} \times \mathcal{Z}}(y, z) = \sum_{i=1}^l \frac{\pi_{\mathbb{R}^m}(x_i)}{\sqrt{\det(\nabla G_i(x_i)^\top \nabla G_i(x_i))}}. \quad (9)$$

where $x_i = G_i^{-1}(y, z)$.

How does theorem 1 relate to the dequantization of smooth manifolds? Manifolds of interest (such the sphere, the torus, or the orthogonal group) can be introduced as elements of a new coordinate system for an ambient Euclidean space. By marginalizing out the other dimensions of the new coordinate system, we obtain the distribution on the manifold of interest. We have already seen an example of this in section 2 where \mathbb{R}^3 was transformed into a spherical coordinate system. We generalize this as follows:

Example 4 (Hypersphere). The hyperspherical coordinate transformation giving the isomorphism of $\mathbb{R}^m \setminus \{0\}$ and $\mathbb{S}^{m-1} \times \mathbb{R}_+$ is defined by, $x \mapsto (x/r, r)$ where $r = \|x\|_2$. The inverse transformation is $(s, r) \mapsto rs$. The Jacobian determinant of the hyperspherical coordinate transformation is $1/r^{m-1}$. Hence, given a density on \mathbb{R}^m (equivalent to

$\mathbb{R}^m \setminus \{0\}$ up to a set of Lebesgue measure zero) we may compute the change-of-variables so as to obtain a density on $\mathbb{S}^{m-1} \times \mathbb{R}_+$ by applying theorem 1 and the fact that the Jacobian determinant of the transformation is $1/r^{m-1}$.

Example 5 (Torus). From the fact that $\mathbb{R}^2 \cong \mathbb{S}^1 \times \mathbb{R}_+$ (a consequence of the polar coordinate transformation), we may similarly develop a coordinate system of even-dimensional Euclidean space in which the torus appears. Recall that $\mathbb{T}^m \cong \mathbb{S}_1 \times \dots \times \mathbb{S}_1$ (there are m terms in the product). Therefore, we have established that

$$\mathbb{R}^{2m} \setminus \{0\} \cong \mathbb{T}^m \times \underbrace{\mathbb{R}_+ \times \dots \times \mathbb{R}_+}_{m \text{ times}}. \quad (10)$$

The isomorphism can be explicitly constructed by writing $x = (x_{1,1}, x_{1,2}, \dots, x_{m,1}, x_{m,2})$ and defining the map $G : \mathbb{R}^{2m} \setminus \{0\} \rightarrow \mathbb{T}^m \times \mathbb{R}_+ \times \dots \times \mathbb{R}_+$ by,

$$G(x) \stackrel{\text{def.}}{=} (x_{1,1}/r_1, \dots, x_{m,1}/r_m, r_1, \dots, r_m), \quad (11)$$

where $r_i = \sqrt{x_{i,1}^2 + x_{i,2}^2}$. As the concatenation of m polar coordinate transformations, the Jacobian determinant of this transformation is $\prod_{i=1}^m r_i^{-1}$. The inverse transformation from $\mathbb{T}^m \times \mathbb{R}_+ \times \dots \times \mathbb{R}_+$ back to $\mathbb{R}^{2m} \setminus \{0\}$ is given by,

$$G^{-1}(s_1, \dots, s_m, r_1, \dots, r_m) = (r_1 s_1, \dots, r_m s_m), \quad (12)$$

where $(s_1, \dots, s_m) \in \mathbb{S}^1 \times \dots \times \mathbb{S}^1 \cong \mathbb{T}^m$. In the case of the torus, the product $\mathbb{R}_+ \times \dots \times \mathbb{R}_+$ is the dequantization dimension of \mathbb{T}^m into $\mathbb{R}^{2m} \setminus \{0\}$. We describe a different means of dequantization, called *modulus dequantization*, in appendix C.

5.1. Stiefel Manifold

The coordinate transformation in which the Stiefel manifold appears requires a more involved construction than was the case for the sphere or torus. Our first result relates the Stiefel manifold, full-rank matrices, and positive definite matrices.

Proposition 1. $FR(n, p) \cong \text{Stiefel}(n, p) \times \text{PD}(p)$.

The isomorphism of these spaces is constructed by the *polar decomposition*. Given $\mathbf{M} \in FR(n, p, \mathbb{R})$, define,

$$\mathbf{P} \stackrel{\text{def.}}{=} \sqrt{\mathbf{M}^\top \mathbf{M}} \in \text{PD}(p) \quad (13)$$

$$\mathbf{O} \stackrel{\text{def.}}{=} \mathbf{M}\mathbf{P}^{-1} \in \text{Stiefel}(n, p). \quad (14)$$

Thus, the isomorphism is given by $\mathbf{M} \mapsto (\mathbf{O}, \mathbf{P})$. This isomorphism is rigorously established in appendix D.

Integrating over $\text{PD}(n)$ may be non-trivial due to the complicated structure of the positive-definite manifold of matrices. However, there is an isomorphism of $\text{PD}(n)$ and $\text{Tri}_+(n)$, the set of $n \times n$ lower-triangular matrices with strictly positive entries on the diagonal. The isomorphism is

given by the Cholesky decomposition: If $\mathbf{P} \in \text{PD}(n)$ then there is a unique matrix $\mathbf{L} \in \text{Tri}_+(n)$ such that $\mathbf{P} = \mathbf{L}\mathbf{L}^\top$. We have therefore proved the following.

Proposition 2. $\text{FR}(n, p) \cong \text{Stiefel}(n, p) \times \text{Tri}_+(p)$.

One can use automatic differentiation in order to compute the Jacobian determinant of the transformation defined by $\mathbf{M} \mapsto (\mathbf{O}, \mathbf{L})$. We call the transformation $\mathbf{M} \mapsto (\mathbf{O}, \mathbf{L})$ the *Cholesky polar decomposition*. The inverse transformation is $(\mathbf{O}, \mathbf{L}) \mapsto \mathbf{OLL}^\top$

The Stiefel manifold $\text{Stiefel}(n, p)$ is a generalization of the orthogonal group $\text{O}(n)$ and we recover the latter exactly when $n = p$. In this case, we identify $\text{FR}(n, n)$ as $\text{GL}(n)$ so that we proved the following.

Corollary 2. $\text{GL}(n) \cong \text{O}(n) \times \text{PD}(n)$.

Finally we observe that almost all $n \times p$ matrices are full-rank. Therefore, if one has a density in $\mathbb{R}^{n \times p}$ then we may apply the polar decomposition coordinate transformation in order to obtain a density on $\text{Stiefel}(n, p) \times \text{PD}(p)$. Here $\text{Tri}_+(p)$ plays the role of the dequantization dimension of $\text{Stiefel}(n, p)$ into $\text{FR}(n, p)$.

5.2. Dequantization

We have now seen how several manifolds appear in coordinate systems. In each case, the manifold appears with an auxiliary manifold which may not be of immediate interest. Namely, (i) The sphere appears with set of positive real numbers when defining a coordinate system for $\mathbb{R}^m \setminus \{0\} \cong \mathbb{S}^{m-1} \times \mathbb{R}_+$; (ii) The torus appears the product manifold of m copies of the positive real numbers when defining a coordinate system for $\mathbb{R}^{2m} \setminus \{0\} \cong \mathbb{T}^m \times \mathbb{R}_+ \times \dots \times \mathbb{R}_+$; (iii) the Stiefel manifold appears with the set of lower-triangular matrices with positive diagonal entries when defining a coordinate system of $\text{FR}(n, p) \cong \text{Stiefel}(n, p) \times \text{Tri}_+(p)$. We would like to marginalize out these “nuisance manifolds” so as to obtain distributions on the manifold of primary interest. A convenient means to achieve this is to introduce an importance sampling distribution over the nuisance manifold. Formally, we have the following result, which is an immediate consequence of theorem 1.

Corollary 3. Let \mathcal{Y} , \mathcal{Z} , G , and $\pi_{\mathcal{Y} \times \mathcal{Z}}$ be as defined in theorem 1. Let $\tilde{\pi}_{\mathcal{Z}}$ be a non-vanishing density on \mathcal{Z} . To obtain the marginal density on \mathcal{Y} , it suffices to compute,

$$\pi_{\mathcal{Y}}(y) = \mathbb{E}_{z \sim \tilde{\pi}_{\mathcal{Z}}(z)} \frac{\pi_{\mathcal{X}}(x)}{\tilde{\pi}_{\mathcal{Z}}(z) \cdot \sqrt{\det(\nabla G(x)^\top \nabla G(x))}}, \quad (15)$$

where $x = G^{-1}(y, z)$.

Let us now consider some examples of marginalizing out the nuisance manifolds in some cases of interest.

Example 6 (Hypersphere). Let $G : \mathbb{R}^m \rightarrow \mathbb{S}^{m-1} \times \mathbb{R}_+$ be the hyperspherical coordinate transformation described

in example 4. Given a density $\pi_{\mathbb{R}^m}$ on \mathbb{R}^m , the manifold change-of-variables formula says that the corresponding density on $\mathbb{S}^{m-1} \times \mathbb{R}_+$ is

$$\pi_{\mathbb{S}^{m-1} \times \mathbb{R}_+}(s, r) = r^{m-1} \cdot \pi_{\mathbb{R}^m}(rs). \quad (16)$$

To obtain the marginal distribution $\pi_{\mathbb{S}^{m-1}}$ we compute,

$$\pi_{\mathbb{S}^{m-1}}(s) = \int_{\mathbb{R}_+} r^{m-1} \cdot \pi_{\mathbb{R}^m}(rs) dr. \quad (17)$$

Or, using an importance sampling distribution $\tilde{\pi}_{\mathbb{R}_+}$ whose support is \mathbb{R}_+ , we obtain,

$$\pi_{\mathbb{S}^{m-1}}(s) = \mathbb{E}_{r \sim \tilde{\pi}_{\mathbb{R}_+}} \frac{r^{m-1} \cdot \pi_{\mathbb{R}^m}(rs)}{\tilde{\pi}_{\mathbb{R}_+}(r)}. \quad (18)$$

Example 7 (Torus). Let G be the toroidal coordinate transformation described in example 5. If one has a density $\pi_{\mathbb{R}^4} : \mathbb{R}^4 \rightarrow \mathbb{R}_+$ then the associated density under the change-of-variables G is $\pi_{\mathbb{T}^2 \times \mathbb{R}_+ \times \mathbb{R}_+}(s_1, s_2, r_1, r_2) = r_1 r_2 \cdot \pi_{\mathbb{R}^4}((r_1 s_1, r_2 s_2))$. Similar to example 6, one can introduce an importance sampling distribution on $\mathbb{R}_+ \times \mathbb{R}_+$ so as to obtain the marginal distribution on the torus:

$$\pi_{\mathbb{T}^2}(s_1, s_2) = \mathbb{E}_{r_1, r_2 \sim \tilde{\pi}_{\mathbb{R}_+} \times \mathbb{R}_+} \frac{\pi_{\mathbb{R}^4}((r_1 s_1, r_2 s_2))}{1/r_1 r_2}. \quad (19)$$

Example 8 (Stiefel Manifold). Let G be the Cholesky polar decomposition coordinate transformation described in section 5.1. Given a density in $\pi_{\mathbb{R}^{n \times p}} : \mathbb{R}^{n \times p} \rightarrow \mathbb{R}_+$, we can construct the corresponding density on $\text{Stiefel}(n, p) \times \text{Tri}_+(p)$ by applying theorem 1:

$$\pi_{\text{Stiefel}(n, p) \times \text{Tri}_+(p)}(\mathbf{O}, \mathbf{L}) = \frac{\pi_{\mathbb{R}^{n \times p}}(\mathbf{OP})}{\mathcal{J}(\mathbf{OP})} \quad (20)$$

where $\mathbf{P} = \mathbf{LL}^\top$ and $\mathcal{J}(\mathbf{OP}) \stackrel{\text{def}}{=} \sqrt{\det((\nabla G(\mathbf{OP}))^\top (\nabla G(\mathbf{OP})))}$. To construct an importance sampling distribution over $\text{Tri}_+(p)$, one could generate the diagonal entries of $\mathbf{L}_{ii} \sim \text{LogNormal}(\mu_i, \sigma_i^2)$ and the remaining entries in the lower triangle according to $\mathbf{L}_{ij} \sim \text{Normal}(\mu_{ij}, \sigma_{ij}^2)$. Applying corollary 3 gives the importance sampling formula for the marginal density on $\text{Stiefel}(n, p)$:

$$\pi_{\text{Stiefel}(n, p)}(\mathbf{O}) = \mathbb{E}_{\mathbf{L} \sim \tilde{\pi}_{\text{Tri}_+}} \frac{\pi_{\mathbb{R}^{n \times p}}(\mathbf{OP})}{\mathcal{J}(\mathbf{OP}) \cdot \tilde{\pi}_{\text{Tri}_+}(\mathbf{L})}. \quad (21)$$

A further example of applying dequantization to the *integers* is given in appendix B.

6. Discussion

We investigate the problem of density estimation given observations on a manifold using the dequantization procedure described in section 5.

Algorithm 1 Training loop for dequantization inference. The target density π_Y is only relevant insofar as we must have samples available from it. The algorithm produces θ and ϕ that parameterize a distribution on \mathbb{R}^m and a dequantization density on \mathcal{Z} . Together, these two densities can be combined to compute an estimate of the density using the right-hand side of eq. (15).

- 1: **Input:** Samples from target density $\mathcal{D} \stackrel{\text{def.}}{=} (y_1, \dots, y_B)$ on an embedded manifold $\mathcal{Y} \subset \mathbb{R}^m$, step-size $\epsilon \in \mathbb{R}$.
- 2: Identify a smooth change-of-variables $G : \mathbb{R}^m \rightarrow \mathcal{Y} \times \mathcal{Z}$ where $\mathcal{Z} \subset \mathbb{R}^p$ is an auxiliary structure.
- 3: Let $\pi_{\mathbb{R}^m}$ be a density on \mathbb{R}^m that is smoothly parameterized by $\theta \in \mathbb{R}^{n_{\text{amb}}}$.
- 4: Let $\tilde{\pi}_{\mathcal{Z}}$ be a density on \mathcal{Z} that is continuously parameterized by $y \in \mathcal{Y}$ and smoothly parameterized by $\phi \in \mathbb{R}^{n_{\text{deq}}}$.
- 5: **while** Not Done **do**
- 6: Use eq. (25) or eq. (26) to compute an average loss over \mathcal{D} :

$$\mathcal{L}(\theta, \phi | \mathcal{D}) = \mathbb{E}_{y \sim \text{Unif}(\mathcal{D})} \mathcal{F}(y | \theta, \phi) \quad (22)$$

where \mathcal{F} is the right-hand side of eq. (25) or eq. (26), respectively.

- 7: Update

$$\theta = \theta - \epsilon \nabla_{\theta} \mathcal{L}(\theta, \phi | \mathcal{D}) \quad (23)$$

$$\phi = \phi - \epsilon \nabla_{\phi} \mathcal{L}(\theta, \phi | \mathcal{D}). \quad (24)$$

- 8: **end while**
- 9: **Output:** Parameterized densities $\pi_{\mathbb{R}^m}(\cdot | \theta)$ and $\tilde{\pi}_{\mathcal{Z}}(\cdot | y, \phi)$ that can be used to perform density estimation on \mathcal{Y} using eq. (15).

Problem. Let \mathcal{Y} be a manifold embedded in \mathbb{R}^n and let π_Y be a density on \mathcal{Y} . Given observations of π_Y , construct an estimate $\hat{\pi}_Y$ of the density π_Y .

Algorithm 1 shows how we may apply dequantization for the purposes of density estimation provided that we have samples from the target density. We apply eq. (15) in order to obtain the density estimate on \mathcal{Y} . Generating samples from π_Y may be achieved by first sampling $x \sim \pi_{\mathcal{X}}$, applying the transformation $G(x) = (y, z)$, and taking y as a sample from the approximated distribution $\hat{\pi}_Y$.

6.1. Densities on \mathbb{R}^m

As \mathbb{R}^m is a Euclidean space, we have available a wealth of possible mechanisms to produce flexible densities in the ambient space. One popular choice is RealNVP (Dinh et al., 2017). In this case θ is the parameters of the underlying RealNVP network. An alternative is neural ODEs wherein θ pa-

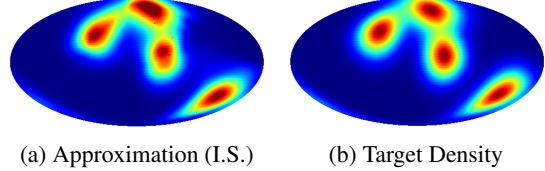


Figure 3. Comparison of the density on \mathbb{S}^2 learned via RealNVP dequantization with a KL-divergence loss estimated via importance sampling. The dequantization procedure is able to identify all modes of the density correctly.

rameterizes a vector field in the Euclidean space; the change in probability density under the vector field flow is obtained by integrating the instantaneous change-of-variables formula (Chen et al., 2018; Grathwohl et al., 2018).

6.2. Objective Functions

We consider two possible objective functions for density estimation. The first is the evidence lower bound of the observations $\{y_1, \dots, y_{n_{\text{obs}}}\}$:

$$\log \hat{\pi}_Y(y_i) \geq \mathbb{E}_{z \sim \tilde{\pi}_{\mathcal{Z}}} \log \frac{\pi_{\mathbb{R}^m}(G^{-1}(y_i, z))}{\tilde{\pi}_{\mathcal{Z}}(z) \cdot \sqrt{\det(\nabla G(x)^\top \nabla G(x))}}. \quad (25)$$

This follows as a consequence of Jensen’s inequality applied to eq. (15). Experimental results using this objective function are denoted with the suffix (ELBO). The second is the log-likelihood computed via importance sampling:

$$\log \hat{\pi}_Y(y_i) = \log \mathbb{E}_{z \sim \tilde{\pi}_{\mathcal{Z}}} \frac{\pi_{\mathbb{R}^m}(G^{-1}(y_i, z))}{\tilde{\pi}_{\mathcal{Z}}(z) \cdot \sqrt{\det(\nabla G(x)^\top \nabla G(x))}}. \quad (26)$$

Because the calculation of eq. (26) requires an importance sampling estimate, experimental results using this objective function are denoted with the suffix (I.S.).

7. Experimental Results

To demonstrate the effectiveness of the approach, we now show experimental results for density estimation on three different manifolds: the sphere, the torus and the orthogonal group. In our comparison against competing algorithms, we ensure that each method has a comparable number of learnable parameters. Our evaluation metrics are designed to test the fidelity of the density estimate to the target distribution; details on evaluation metrics are given in appendix G. In all of our examples we use rejection sampling in order to draw samples from the target distribution.

7.1. Sphere and Hypersphere

Our first experimental results concern the sphere \mathbb{S}^2 where we consider a multimodal distribution with four modes.

Table 1. Comparison of dequantization to normalizing flows on the multimodal density on \mathbb{S}^2 . Averages were computed using ten random trials for the dequantization procedures and eight random trials for the normalizing flow (because two random trials exhibited divergent behavior and were excluded). The dequantization procedure is illustrated for both the ELBO loss and the KL divergence loss.

Method	Mean MSE	Covariance MSE	$\text{KL}(q\ p)$	$\text{KL}(p\ q)$	Relative ESS
Deq. ODE (ELBO)	0.0012 ± 0.0002	0.0006 ± 0.0001	0.0046 ± 0.0002	0.0046 ± 0.0002	99.0990 ± 0.0401
Deq. ODE (I.S.)	0.0014 ± 0.0002	0.0010 ± 0.0001	0.0029 ± 0.0001	0.0029 ± 0.0001	99.4170 ± 0.0225
Deq. RealNVP (ELBO)	0.0004 ± 0.0001	0.0003 ± 0.0001	0.0231 ± 0.0010	0.0212 ± 0.0009	95.9540 ± 0.1688
Deq. RealNVP (I.S.)	0.0005 ± 0.0002	0.0002 ± 0.0000	0.0124 ± 0.0006	0.0115 ± 0.0006	97.8240 ± 0.1183
Man. ODE	0.0010 ± 0.0004	0.0009 ± 0.0002	0.0085 ± 0.0007	0.0083 ± 0.0007	98.3860 ± 0.1328
Möbius	0.0021 ± 0.0005	0.0019 ± 0.0005	0.0595 ± 0.0025	—	89.2575 ± 0.4888

Table 2. Comparison of dequantization to normalizing flows on the multimodal density on \mathbb{S}^3 . Averages were computed using ten random trials for the dequantization procedures and nine random trials for the normalizing flow (one random trial exhibited divergent behavior and was excluded).

Method	Mean MSE	Covariance MSE	$\text{KL}(q\ p)$	$\text{KL}(p\ q)$	Relative ESS
Deq. ODE (ELBO)	0.0009 ± 0.0001	0.0007 ± 0.0001	0.0072 ± 0.0002	0.0070 ± 0.0002	98.6490 ± 0.0388
Deq. ODE (I.S.)	0.0017 ± 0.0001	0.0022 ± 0.0002	0.0189 ± 0.0004	0.0180 ± 0.0004	96.6150 ± 0.0648
Deq. RealNVP (ELBO)	0.0003 ± 0.0001	0.0004 ± 0.0001	0.0384 ± 0.0010	0.0283 ± 0.0005	95.1880 ± 0.0771
Deq. RealNVP (I.S.)	0.0003 ± 0.0001	0.0003 ± 0.0000	0.0208 ± 0.0004	0.0180 ± 0.0004	96.6340 ± 0.0920
Man. ODE	0.0012 ± 0.0003	0.0008 ± 0.0002	0.0098 ± 0.0009	0.0094 ± 0.0007	98.1780 ± 0.1302
Möbius	0.0027 ± 0.0004	0.0014 ± 0.0003	0.0542 ± 0.0047	—	88.7290 ± 0.9332

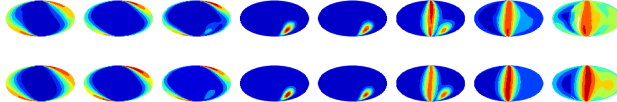


Figure 4. Comparison of the density on \mathbb{S}^3 learned via RealNVP dequantization with a KL-divergence loss. We visualize \mathbb{S}^2 -slices of \mathbb{S}^3 by examining the density when one of the hyperspherical coordinates is held fixed. The top set of slices shows the approximate density obtained via dequantization and the target density. The KL divergence is 0.01269 and the relative effective sample size is 97.70%.

This density on \mathbb{S}^2 which is visualized in fig. 3. We consider performing density estimation using the ELBO (eq. (25)) and log-likelihood objective functions (eq. (26)); we construct densities in the ambient space using RealNVP and neural ODEs. We use algorithm 1 to learn the parameters of the ambient and dequantization distributions. As baselines we consider the Möbius transform approach described in (Rezende et al., 2020), which is a specialized normalizing flow method for tori and spheres, and the neural manifold ODE applied to the sphere as described in (Lou et al., 2020). We give a comparison of performance metrics between these methods in table 1. In these experiments, we find that parameterizing a neural ODE model in the ambient space gave the better KL-divergence and effective sample size (ESS) metrics than RealNVP when our dequantization approach is used. We find that our dequantization algorithm minimizing either eq. (25) or eq. (26) achieves similar performance in

the first and second moment metrics. However, when using eq. (26), slightly lower KL-divergence metrics are achievable as well as slightly larger effective sample sizes. In either case, dequantization tends to outperform the Möbius transform on this multimodal density on \mathbb{S}^2 . The manifold ODE method is outperformed by the ODE dequantization algorithms with both eq. (25) and eq. (26).

We next consider a multimodal density $\mathbb{S}^3 \cong \text{SU}(3)$ (the special unitary group). We visualize \mathbb{S}^2 -slices of this density in fig. 4. As before, we compare dequantization to Möbius flow transformations and manifold neural ODEs and present results in table 2. Similar to the case of the multimodal density on \mathbb{S}^2 , we find that dequantization with an ambient neural ODE model is most effective, with ELBO maximization giving the smallest KL-divergence metrics. All dequantization algorithms out-performed the Möbius transformation on the sphere but only dequantization with an ambient ODE and ELBO minimization outperformed the manifold neural ODE method.

7.2. Torus

We next consider three densities from (Rezende et al., 2020) on the torus \mathbb{T}^2 . These densities are, respectively, unimodal, multimodal, or exhibit strongly correlated dimensions. As in section 7.1, we evaluate dequantization of the torus against the Möbius transform method. As a further point of comparison, we also consider learning a normalizing flow density on \mathbb{R}^2 and simply identifying every 2π -periodic point so as to induce distribution on \mathbb{T}^2 ; we call this the modulus

Table 3. Comparison of Deq. RealNVP to Möbius Flow flows on the multimodal density on \mathbb{T}^2 . Averages were computed using ten random trials for the Deq. RealNVP procedures, direct, and Möbius Flow flow procedures.

Density	Method	Mean MSE	Covariance MSE	$KL(q\ p)$	$KL(p\ q)$	Relative ESS
Correlated	Deq. RealNVP (ELBO)	0.0019 \pm 0.0007	0.0098 \pm 0.0019	0.0072 \pm 0.0005	0.0084 \pm 0.0006	98.6510 \pm 0.0958
	Deq. RealNVP (I.S.)	0.0024 \pm 0.0007	0.0121 \pm 0.0041	0.0038 \pm 0.0004	0.0040 \pm 0.0004	99.2570 \pm 0.0796
	Modulus	0.0017 \pm 0.0005	0.0072 \pm 0.0021	0.0025 \pm 0.0006	0.0025 \pm 0.0006	99.5000 \pm 0.1153
	Möbius	0.0004 \pm 0.0002	0.0083 \pm 0.0029	0.0021 \pm 0.0002	—	99.5850 \pm 0.0332
Unimodal	Deq. RealNVP (ELBO)	0.0010 \pm 0.0003	0.0133 \pm 0.0040	0.0066 \pm 0.0004	0.0079 \pm 0.0004	98.7240 \pm 0.0761
	Deq. RealNVP (I.S.)	0.0011 \pm 0.0003	0.0081 \pm 0.0020	0.0021 \pm 0.0002	0.0023 \pm 0.0002	99.5980 \pm 0.0317
	Modulus	0.0014 \pm 0.0003	0.0164 \pm 0.0028	0.0028 \pm 0.0003	0.0028 \pm 0.0003	99.4340 \pm 0.0531
	Möbius	0.0006 \pm 0.0002	0.0055 \pm 0.0037	0.0008 \pm 0.0001	—	99.8490 \pm 0.0293
Multimodal	Deq. RealNVP (ELBO)	0.0024 \pm 0.0006	0.0158 \pm 0.0026	0.0065 \pm 0.0002	0.0075 \pm 0.0002	98.7800 \pm 0.0379
	Deq. RealNVP (I.S.)	0.0007 \pm 0.0002	0.0061 \pm 0.0014	0.0020 \pm 0.0001	0.0022 \pm 0.0002	99.6160 \pm 0.0288
	Modulus	0.0016 \pm 0.0007	0.0063 \pm 0.0024	0.0035 \pm 0.0004	0.0035 \pm 0.0004	99.3030 \pm 0.0725
	Möbius	0.0006 \pm 0.0001	0.0070 \pm 0.0039	0.0012 \pm 0.0002	—	99.7600 \pm 0.0358

Table 4. Metrics of the dequantization algorithm in application to the orthogonal Procrustes problem and dequantization of a multimodal density on $SO(3)$. Results are averaged over ten independent trials for the multimodal distribution on $SO(3)$ and nine independent trials for the orthogonal Procrustes problem.

Experiment	Mean MSE	Covariance MSE	$KL(q\ p)$	$KL(p\ q)$	Relative ESS
Procrustes (ELBO)	0.0021 \pm 0.0008	0.0012 \pm 0.0005	0.0193 \pm 0.0069	0.0173 \pm 0.0053	96.9489 \pm 0.7649
Procrustes (I.S.)	0.0038 \pm 0.0020	0.0015 \pm 0.0008	0.0301 \pm 0.0126	0.0202 \pm 0.0075	95.6944 \pm 1.4654
$SO(3)$ (ELBO)	0.0007 \pm 0.0002	0.0029 \pm 0.0003	0.0443 \pm 0.0011	0.0415 \pm 0.0059	96.2930 \pm 0.0649
$SO(3)$ (I.S.)	0.0004 \pm 0.0001	0.0014 \pm 0.0001	0.0207 \pm 0.0028	0.0235 \pm 0.0029	97.7280 \pm 0.1136

dequantization method. Results are reported in table 3. We find that the Möbius transformation performs strongest in this comparison. The modulus method also performs well, particularly on the correlated toroidal density function. Of the dequantization-based approaches, minimizing the negative log-likelihood produces the best performance, which outperforms the modulus method in terms of KL-divergence and first- and second-moment metrics (excepting the correlated density). We note, however, that all of these methods estimated effective sample sizes at nearly 100%, indicating that the differences between each approach, while statistically significant, are practically marginal.

7.3. Orthogonal Group

The previous two examples focused on manifolds composed of spheres and circles. We now examine density estimation on the orthogonal group, where we consider inference in a probabilistic variant of the orthogonal Procrustes problem; we seek to sample orthogonal transformations that transport one point cloud towards another in terms of squared distance. We consider parameterizing a distribution in the ambient Euclidean space using RealNVP in these experiments. Results are presented in table 4. We observe that optimizing the ELBO objective function (eq. (25)) tended to produce better density estimates than the log-likelihood (eq. (26)). Nevertheless, we find that either dequantization algorithm is highly effective at matching the target density.

We may also leverage corollary 1 so as to apply our method to the “dequantization” of $SO(n)$. As an example, we consider a multimodal density on $SO(3)$. Results of applying our method to sampling from this distribution are also shown in table 4. In this example we find that minimizing the negative log-likelihood using importance sampling tended to produce the best approximation of the first- and second-moments of the distribution, in addition to smaller KL-divergence metrics.

8. Conclusion

This paper proposed a new method for density estimation on manifolds called manifold dequantization. The proposed approach allows us to make use of existing techniques for density estimation on Euclidean spaces while still providing efficient, exact sampling of the distribution on the manifold as well as approximate density calculation. We evaluated this method for densities on the sphere, the torus, and the orthogonal group. Our results show that manifold dequantization is competitive with, or exceeds the performance of, competing methods for density estimation on manifolds.

Acknowledgments

This material is based upon work supported by the National Science Foundation Graduate Research Fellowship under Grant No. 1752134. Any opinion, findings, and conclusions or recommendations expressed in this material are those

of the authors(s) and do not necessarily reflect the views of the National Science Foundation. The contributions of MAB in this work was undertaken as part of the Vision: Science to Applications program, thanks in part to funding from the Canada First Research Excellence Fund. RRL was supported in part by NIH/NIGMS 1R01GM136780-01.

References

Bose, J., Smofsky, A., Liao, R., Panangaden, P., and Hamilton, W. Latent variable modelling with hyperbolic normalizing flows. In III, H. D. and Singh, A. (eds.), *Proceedings of the 37th International Conference on Machine Learning*, volume 119 of *Proceedings of Machine Learning Research*, pp. 1045–1055. PMLR, 13–18 Jul 2020. URL <http://proceedings.mlr.press/v119/bose20a.html>.

Brubaker, M., Salzmann, M., and Urtasun, R. A family of mcmc methods on implicitly defined manifolds. In Lawrence, N. D. and Girolami, M. (eds.), *Proceedings of the Fifteenth International Conference on Artificial Intelligence and Statistics*, volume 22 of *Proceedings of Machine Learning Research*, pp. 161–172, La Palma, Canary Islands, 21–23 Apr 2012. PMLR. URL <http://proceedings.mlr.press/v22/brubaker12.html>.

Chen, R. T. Q., Rubanova, Y., Bettencourt, J., and Duvenaud, D. K. Neural ordinary differential equations. In Bengio, S., Wallach, H., Larochelle, H., Grauman, K., Cesa-Bianchi, N., and Garnett, R. (eds.), *Advances in Neural Information Processing Systems*, volume 31, pp. 6571–6583. Curran Associates, Inc., 2018. URL <https://proceedings.neurips.cc/paper/2018/file/69386f6bb1dfed68692a24c8686939b9-Paper.pdf>.

Dinh, L., Sohl-Dickstein, J., and Bengio, S. Density estimation using real NVP. In *5th International Conference on Learning Representations, ICLR 2017, Toulon, France, April 24-26, 2017, Conference Track Proceedings*. OpenReview.net, 2017. URL <https://openreview.net/forum?id=HkpbnH9lx>.

Doucet, A., Smith, A., de Freitas, N., and Gordon, N. *Sequential Monte Carlo Methods in Practice*. Information Science and Statistics. Springer New York, 2001. ISBN 9780387951461. URL <https://books.google.com/books?id=uxX-koqKtMMC>.

Falorsi, L., de Haan, P., Davidson, T. R., and Forré, P. Reparameterizing distributions on lie groups. volume 89 of *Proceedings of Machine Learning Research*, pp. 3244–3253. PMLR, 16–18 Apr 2019. URL <http://proceedings.mlr.press/v89/falorsi19a.html>.

Federer, H. *Geometric Measure Theory*. Die Grundlehren der mathematischen Wissenschaften in Einzeldarstellungen. Springer, 1969. ISBN 9780387045054. URL <https://books.google.com/books?id=TALvAAAAMAAJ>.

Gower, J. C. and Dijksterhuis, G. B. *Procrustes Problems*. Oxford University Press, 2004. ISBN 9780198510581.

Grathwohl, W., Chen, R. T. Q., Bettencourt, J., Sutskever, I., and Duvenaud, D. Ffjord: Free-form continuous dynamics for scalable reversible generative models, 2018.

Ho, J., Chen, X., Srinivas, A., Duan, Y., and Abbeel, P. Flow++: Improving flow-based generative models with variational dequantization and architecture design, 2019.

Hoogeboom, E., Cohen, T. S., and Tomczak, J. M. Learning discrete distributions by dequantization, 2020.

Jones, F. Integration on manifolds, 2004. URL <http://www.owlnet.rice.edu/%7Efjones/chap11.pdf>.

Kobyzev, I., Prince, S., and Brubaker, M. Normalizing flows: An introduction and review of current methods. *IEEE Transactions on Pattern Analysis and Machine Intelligence*, 2020.

Lee, J. *Introduction to Smooth Manifolds*. Graduate Texts in Mathematics. Springer, 2003. ISBN 9780387954486. URL <https://books.google.com/books?id=eqfgZtjQceYC>.

Lippe, P. and Gavves, E. Categorical normalizing flows via continuous transformations, 2021.

Liu, J. S. *Monte Carlo Strategies in Scientific Computing*. Springer Publishing Company, Incorporated, 2008. ISBN 0387763694.

Lou, A., Lim, D., Katsman, I., Huang, L., Jiang, Q., Lim, S.-N., and De Sa, C. Neural manifold ordinary differential equations. *arXiv preprint arXiv:2006.10254*, 2020.

Papamakarios, G., Nalisnick, E., Rezende, D. J., Mohamed, S., and Lakshminarayanan, B. Normalizing flows for probabilistic modeling and inference, 2019.

Rezende, D. J., Papamakarios, G., Racanière, S., Albergo, M. S., Kanwar, G., Shanahan, P. E., and Cranmer, K. Normalizing flows on tori and spheres. *CoRR*, abs/2002.02428, 2020. URL <https://arxiv.org/abs/2002.02428>.

Theis, L., van den Oord, A., and Bethge, M. A note on the evaluation of generative models, 2016.

Uria, B., Murray, I., and Larochelle, H. Rnade: The real-valued neural autoregressive density-estimator. *arXiv preprint arXiv:1306.0186*, 2013.

Wang, F. and Gelfand, A. E. Directional data analysis under the general projected normal distribution. *Statistical Methodology*, 10(1):113 – 127, 2013. ISSN 1572-3127. doi: <https://doi.org/10.1016/j.stamet.2012.07.005>. URL <http://www.sciencedirect.com/science/article/pii/S1572312712000457>.

A. Evidence Lower Bound for $\text{SO}(n)$

$$\log \pi_{\text{SO}(n)}(\mathbf{O}) = \log \mathbb{E}_{\mathbf{S} \sim \text{Unif}(\text{Id}_n, \mathbf{R})} \pi_{\text{O}(n)}(\mathbf{SO}) + \log 2 \quad (27)$$

$$\geq \mathbb{E}_{\mathbf{S} \sim \text{Unif}(\text{Id}_n, \mathbf{R})} \log \pi_{\text{O}(n)}(\mathbf{SO}) + \log 2 \quad (28)$$

$$\geq \mathbb{E}_{\mathbf{S} \sim \text{Unif}(\text{Id}_n, \mathbf{R})} \mathbb{E}_{\mathbf{L} \sim \tilde{\pi}_{\text{Tri}_+}} \frac{\pi_{\mathbb{R}^{n \times n}}(\mathbf{SOP})}{\mathcal{J}(\mathbf{OP}) \cdot \tilde{\pi}_{\text{Tri}_+}(\mathbf{L})} + \log 2 \quad (29)$$

$$\geq \mathbb{E}_{\mathbf{S} \sim \text{Unif}(\text{Id}_n, \mathbf{R})} \mathbb{E}_{\mathbf{L} \sim \tilde{\pi}_{\text{Tri}_+}} \frac{\pi_{\mathbb{R}^{n \times n}}(\mathbf{SOP})}{\mathcal{J}(\mathbf{OP}) \cdot \tilde{\pi}_{\text{Tri}_+}(\mathbf{L})} \quad (30)$$

where $\mathcal{J}(\mathbf{OP}) \stackrel{\text{def}}{=} \sqrt{\det((\nabla G(\mathbf{OP}))^\top (\nabla G(\mathbf{OP})))}$.

B. Dequantizing the Integers

We now consider how to apply corollary 1 and theorem 1 to the dequantization of integers and draw a connection to dequantization in normalizing flows (Hoogeboom et al., 2020). Let $\pi_{\mathbb{R}}$ be a probability density on \mathbb{R} . Consider the function $T : \mathbb{R} \rightarrow \mathbb{Z} \times [0, 1)$ defined by $T(x) = (\lfloor x \rfloor, x - \lfloor x \rfloor)$. Consider the partition of \mathbb{R} given by $\mathcal{O}_n = [n, n+1)$; on each \mathcal{O}_n we have that $T_n(x) \stackrel{\text{def.}}{=} (n, x - n)$ satisfies $T_n = T|_{\mathcal{O}_n}$; moreover, on each \mathcal{O}_n , the transformation T_n is invertible (the inverse map is $(n, r) \mapsto n + r$) and preserves volume, which implies a unit Jacobian determinant. Therefore, the associated density on $\mathbb{Z} \times [0, 1)$ is given by $\pi_{\mathbb{Z} \times [0, 1)}(n, r) = \pi_{\mathbb{R}}(n + r)$. We may view $\mathbb{Z} \times [0, 1)$ as a coordinate system for \mathbb{R} . If we wish to integrate out the nuisance variables in the unit interval, we obtain the marginal density on \mathbb{Z} as

$$\pi_{\mathbb{Z}}(n) = \int_0^1 \pi_{\mathbb{R}}(n + r) \, dr. \quad (31)$$

By choosing $\tilde{\pi}_{[0,1]}$ as, for example, a Uniform distribution, one obtains the traditional uniform dequantization. Choosing a more complex distribution, for example, a Beta distribution (with parameters possibly depending on n) one obtains an importance sampling formula for the marginal density as $\pi_{\mathbb{Z}}(n) = \mathbb{E}_{r \sim \tilde{\pi}_{[0,1]}(r)} \frac{\pi_{\mathbb{R}}(n+r)}{\tilde{\pi}_{[0,1]}(r)}$. This can be optimized through a variational bound, giving variational dequantization (Ho et al., 2019). Optimizing it directly gives importance weighted dequantization (Hoogeboom et al., 2020).

C. Torus Modulus Dequantization

Taking inspiration from appendix B, we turn now to consider another dequantization of the torus. To begin, identify the circle \mathbb{S}^1 with the interval $[0, 2\pi]$. We can construct a map from \mathbb{R} to $\mathbb{Z} \times [0, 2\pi]$ by identifying 2π -periodic points. Define the map $\tilde{G}(x) = (\lfloor x \rfloor, x \pmod{2\pi})$. Let $\mathcal{O}_k = [2\pi k, 2\pi(k+1))$ for $k \in \mathbb{Z}$; on this interval we may define $G_k : \mathcal{O}_k \rightarrow \mathbb{Z} \times [0, 2\pi)$ by $G_k(x) = (k, x - 2\pi k)$ which satisfies $G|_{\mathcal{O}_k} = G_k$. Because this map is nothing but a shift by $2\pi k$, it is invertible and volume preserving. Moreover, we may view $\mathbb{Z} \times [0, 2\pi)$ as a coordinate system for \mathbb{R} . Let $\pi_{\mathbb{R}}$ be a density on \mathbb{R} and let $x \sim \pi_{\mathbb{R}}$. The associated density on $\mathbb{Z} \times [0, 2\pi)$ is therefore,

$$\pi_{\mathbb{Z} \times [0, 2\pi)}(k, y) = \pi_{\mathbb{R}}(y + 2\pi k). \quad (32)$$

We may marginalize out the integers to obtain the density on $[0, 2\pi)$ as

$$\pi_{[0, 2\pi)}(y) = \sum_{k \in \mathbb{Z}} \pi_{\mathbb{R}}(y + 2\pi k). \quad (33)$$

This idea is readily extended to higher dimensions. Because the torus is nothing but the product manifold of two circles, we may identify the torus with $[0, 2\pi) \times [0, 2\pi)$. Let $\pi_{\mathbb{R}^2}$ be a density on \mathbb{R}^2 and let $G : \mathbb{R}^2 \rightarrow [\mathbb{Z} \times [0, 2\pi)]^2$ be defined by $G(x_1, x_2) = (\tilde{G}(x_1), \tilde{G}(x_2))$. Following the precise reasoning from the one-dimensional case, if $x \sim \pi_{\mathbb{R}^2}$ then the density of $(x_1 \pmod{2\pi}, x_2 \pmod{2\pi})$ is,

$$\pi_{[0, 2\pi) \times [0, 2\pi)}(y_1, y_2) = \sum_{k_1 \in \mathbb{Z}} \sum_{k_2 \in \mathbb{Z}} \pi_{\mathbb{R}^2}(y_1 + 2\pi k_1, y_2 + 2\pi k_2). \quad (34)$$

We call this approach *modulus dequantization*. This approach requires fewer dimensions than embedding the torus in \mathbb{R}^{2m} . In practice, the infinite sums over the integers may be approximated by truncating to a finite number of terms.

D. Polar Decomposition Isomorphism

Proposition 3. Let \mathbf{A} be a real, positive semi-definite matrix. Then there exists a unique real, positive semi-definite matrix \mathbf{B} such that $\mathbf{A} = \mathbf{B}\mathbf{B}$. We call \mathbf{B} the principal square root of \mathbf{A} and may write $\mathbf{B} = \sqrt{\mathbf{A}}$.

Definition 1 (Stiefel Manifold). The Stiefel(m, n) manifold is the subset of $\mathbb{R}^{m \times n}$ of orthogonal matrices. That is,

$$\text{Stiefel}(m, n) = \{\mathbf{X} \in \mathbb{R}^{m \times n} : \mathbf{X}^\top \mathbf{X} = \text{Id}\} \quad (35)$$

Definition 2. The set of $n \times n$ positive-definite matrices is denoted $\text{PD}(n)$.

Definition 3 (Non-Square Polar Decomposition). Let $\mathbf{A} \in \mathbb{R}^{m \times n}$ with $m \geq n$ have the (thin) singular value decomposition $\mathbf{A} = \mathbf{U}\Sigma\mathbf{V}^\top$ where $\mathbf{U} \in \text{Stiefel}(m, n)$ and $\mathbf{V}^\top \in \text{O}(n)$. Then we define the non-square polar decomposition to be $\mathbf{A} = \mathbf{OP}$ where,

$$\mathbf{O} \stackrel{\text{def}}{=} \mathbf{U}\mathbf{V}^\top \quad (36)$$

$$\mathbf{P} \stackrel{\text{def}}{=} \mathbf{V}\Sigma\mathbf{V}^\top. \quad (37)$$

Lemma 1. The quantity \mathbf{P} in eq. (37) is uniquely defined.

Proof. The strategy is to show that \mathbf{P} is the unique principal square root of a positive semi-definite matrix. It is immediately clear from the definition that \mathbf{P} is itself positive semi-definite. Consider the positive semi-definite matrix

$$\mathbf{A}^\top \mathbf{A} = (\mathbf{V}\Sigma\mathbf{U}^\top)(\mathbf{U}\Sigma\mathbf{V}^\top) \quad (38)$$

$$= \mathbf{V}\Sigma\Sigma\mathbf{V}^\top \quad (39)$$

$$= (\mathbf{V}\Sigma\mathbf{V}^\top)(\mathbf{V}\Sigma\mathbf{V}^\top) \quad (40)$$

$$= \mathbf{P}\mathbf{P}. \quad (41)$$

By identification \mathbf{P} is the principal square root of $\mathbf{A}^\top \mathbf{A}$ so it is unique. \square

Proposition 4. Let $\Sigma = \text{diag}(\sigma_1, \dots, \sigma_n)$ and suppose that $\sigma_1 \geq \sigma_2 \geq \dots \geq \sigma_n > 0$. Then, the quantity \mathbf{O} in eq. (36) is uniquely defined.

Proof. If $\sigma_n > 0$ then

$$\det(\mathbf{P}) = \det(\mathbf{V}) \cdot \det(\Sigma) \cdot \det(\mathbf{V}^\top) \quad (42)$$

$$= \prod_{i=1}^n \sigma_i \quad (43)$$

$$> 0. \quad (44)$$

Thus, \mathbf{P} is invertible. Thus, $\mathbf{O} = \mathbf{AP}^{-1}$. \square

Note that the condition on the singular values is equivalent to the statement that \mathbf{A} has full-rank.

Lemma 2. If \mathbf{A} has full-rank then $\mathbf{P} \in \text{PD}(n)$.

Proof. If \mathbf{A} has full-rank then all the singular values are strictly positive. Thus, $\mathbf{V}\Sigma\mathbf{V}^\top$ is an eigen-decomposition of \mathbf{P} whose eigenvalues are all positive. Since a matrix is positive-definite if and only if all of its eigenvalues are positive, we conclude that $\mathbf{P} \in \text{PD}(n)$. \square

Lemma 3. The quantity \mathbf{O} in eq. (36) is an element of $\text{Stiefel}(m, n)$.

Proof.

$$\mathbf{O}^\top \mathbf{O} = \mathbf{V}\mathbf{U}^\top \mathbf{U}\mathbf{V}^\top \quad (45)$$

$$= \mathbf{V}\mathbf{V}^\top \quad (46)$$

$$= \text{Id}. \quad (47)$$

\square

Proposition 5. Given $\mathbf{O} \in \text{Stiefel}(m, n)$ and $\mathbf{P} \in \text{PD}(n)$, we may always write \mathbf{O} and \mathbf{P} in the form of eqs. (36) and (37).

Proof. Since $\mathbf{P} \in \text{PD}(n)$, by the spectral theorem there exists an orthonormal basis $\{v_1, \dots, v_n\}$ of \mathbb{R}^n and real, positive eigenvalues $\lambda_1, \dots, \lambda_n$, such that $\mathbf{P} = \mathbf{V}\Sigma\mathbf{V}^{-1} = \mathbf{V}\Sigma\mathbf{V}^\top$ where $\mathbf{V} \in \mathbb{R}^{n \times n}$ is the collection of $\{v_1, \dots, v_n\}$ as columns and $\Sigma = \text{diag}(\lambda_1, \dots, \lambda_n)$.

Using this \mathbf{V} we may compute $\mathbf{U} = \mathbf{O}\mathbf{V}$, which is an orthogonal matrix:

$$\mathbf{U}^\top \mathbf{U} = \mathbf{V}^\top \mathbf{O}^\top \mathbf{O} \mathbf{V} \quad (48)$$

$$= \mathbf{V}^\top \mathbf{V} \quad (49)$$

$$= \text{Id.} \quad (50)$$

Define the matrix $\mathbf{A} = \mathbf{O}\mathbf{P}$. By inspection, a (thin) singular value decomposition of \mathbf{A} is

$$\mathbf{A} = \mathbf{U}\Sigma\mathbf{V}^\top \quad (51)$$

since

$$\mathbf{O}\mathbf{P} = \mathbf{U}\mathbf{V}^\top \mathbf{V}\Sigma\mathbf{V}^\top \quad (52)$$

$$= \mathbf{U}\Sigma\mathbf{V}^\top. \quad (53)$$

Finally, $\mathbf{U} \in \text{Stiefel}(m, n)$, Σ has only positive entries, and $\mathbf{V} \in \text{O}(n)$, which are the conditions of a thin singular value decomposition. \square

E. Experimental Details

Here we include additional information about our experimental design.

E.1. Sphere

We consider the following unnormalized density on \mathbb{S}^2 given by

$$\pi_{\mathbb{S}^2}(y) \propto \sum_{i=1}^4 \exp(10y^\top \mu_i) \quad (54)$$

where $\mu_1 = (0.763, 0.643, 0.071)$, $\mu_2 = (0.455, -0.708, 0.540)$, $\mu_3 = (0.396, 0.271, 0.878)$, and $\mu_4 = (-0.579, 0.488, -0.654)$.

When using RealNVP, the total number of learnable parameters in our dequantization model is 5,894; dequantization with an ambient ODE has 5,705 learnable parameters; in the case of the Möbius transform the total number of learnable parameters is 5,943; for the manifold ODE implementation, we have 5,533 parameters.

On \mathbb{S}^3 , we consider an unnormalized density proportional to

$$\pi_{\mathbb{S}^3}(y) \propto \sum_{i=1}^4 \exp(10y^\top \mu_i) \quad (55)$$

$$\mu_1 = (-0.129, 0.070, 0.659, -0.738) \quad (56)$$

$$\mu_2 = (-0.990, -0.076, 0.118, -0.017) \quad (57)$$

$$\mu_3 = (0.825, -0.484, 0.061, 0.285) \quad (58)$$

$$\mu_4 = (-0.801, 0.592, -0.024, 0.081). \quad (59)$$

When using RealNVP, the total number of learnable parameters in our dequantization model is 21,854; dequantization with an ambient ODE has 21,386 learnable parameters; in the case of the Möbius transform the total number of learnable parameters is 25,406; for the manifold ODE implementation, we have 21,204 parameters. For dequantization we use 100 samples per batch and use rejection sampling to draw samples from the unnormalized target density at each iteration.

E.2. Torus

Expressed in terms of their *angular* coordinates (as opposed to their embedding into \mathbb{R}^4), the densities on the torus are as follows:

Unimodal $\pi_{\mathbb{T}^2}^{\text{uni}}(\theta_1, \theta_2 | \phi) \propto \exp(\cos(\theta_1 - \phi_1) + \cos(\theta_2 - \phi_2))$ with $\phi = (4.18, 5.96)$.

Multimodal $\pi_{\mathbb{T}^2}^{\text{mul}}(\theta_1, \theta_2) \propto \sum_{i=1}^3 \pi_{\mathbb{T}^2}^{\text{uni}}(\theta_1, \theta_2 | \phi_i)$ where $\phi_1 = (0.21, 2.85)$, $\phi_2 = (1.89, 6.18)$, and $\phi_3 = (3.77, 1.56)$.

Correlated $\pi_{\mathbb{T}^2}^{\text{cor}}(\theta_1, \theta_2) \propto \exp(\cos(\theta_1 + \theta_2 - 1.94))$.

The number of learnable parameters in the dequantization models is 6,106; in the Möbius flow model, the number of learnable parameters is 5,540; for the direct method, the number of learnable parameters is 5,406. For dequantization we use 100 samples per batch and use rejection sampling to draw samples from the unnormalized target density at each iteration.

E.3. Orthogonal Group

Drawing inspiration from the orthogonal Procrustes problem, we define the unnormalized density by

$$\pi_{\text{O}(n)}(\mathbf{O}) \propto \exp\left(-\frac{1}{2\sigma^2} \|\mathbf{B} - \mathbf{O}\mathbf{A}\|_{\text{fro}}^2\right), \quad (60)$$

where $\mathbf{A}, \mathbf{B} \in \mathbb{R}^{n \times p}$. Given samples from eq. (60), we may apply our dequantization procedure to perform density estimation. In our experiments we take $p = 10$ and $n = 3$. For dequantization we use rejection sampling to draw samples from the posterior. Then, with these fixed samples, we use batches of 100 samples to train the ambient and dequantization distributions.

E.4. $\text{SO}(3)$

Let $\mathbf{R} \in \mathbb{R}^{n \times n}$ be a reflection matrix and notice that $\{\text{SO}(n), \mathbf{RSO}(n)\}$ is partition of $\text{O}(n)$. Given a density on $\mathbb{R}^{n \times n}$, using the methods described in section 5.1, we may obtain a density on $\text{O}(n)$. Then, we define the function $S : \text{O}(n) \rightarrow \text{SO}(n)$ by

$$S(\mathbf{O}) \stackrel{\text{def.}}{=} \begin{cases} \mathbf{O} & \text{if } \det(\mathbf{O}) = +1 \\ \mathbf{R}\mathbf{O} & \text{if } \det(\mathbf{O}) = -1 \end{cases}, \quad (61)$$

where \mathbf{R} is a reflection matrix. Now, define $S_1(\mathbf{O}) \stackrel{\text{def.}}{=} \mathbf{O}$ and $S_2(\mathbf{O}) \stackrel{\text{def.}}{=} \mathbf{R}\mathbf{O}$, which satisfy $S_1 = S|_{\text{SO}(n)}$ and $S_2 = S|_{\mathbf{RSO}(n)}$. Both S_1 and S_2 are self-inverse and volume-preserving maps on their respective domains so we may obtain a density on $\text{SO}(n)$ as

$$\pi_{\text{SO}(n)}(\mathbf{O}) = \pi_{\text{O}(n)}(\mathbf{O}) + \pi_{\text{O}(n)}(\mathbf{R}\mathbf{O}). \quad (62)$$

One may immediately seek to minimize the negative log-likelihood of data using eq. (62). Alternatively, we use the following ELBO in our experiments:

$$\log \pi_{\text{SO}(n)}(\mathbf{O}) \geq \mathbb{E}_{\mathbf{S} \sim \text{Unif}(\text{Id}_n, \mathbf{R})} \mathbb{E}_{\mathbf{L} \sim \tilde{\pi}_{\text{Tri}_+}} \frac{\pi_{\mathbb{R}^{n \times n}}(\mathbf{SOP})}{\det(\nabla G(\mathbf{SOP})) \cdot \tilde{\pi}_{\text{Tri}_+}(\mathbf{L})}, \quad (63)$$

where, as in example 8, $\mathbf{P} = \mathbf{L}\mathbf{L}^\top$. For a short derivation of this ELBO, see appendix A.

We consider the following multimodal density on $\text{SO}(3)$:

$$\pi_{\text{SO}(3)}(\mathbf{O}) \propto \sum_{i=1}^3 \exp\left(-\frac{1}{2\sigma^2} \|\mathbf{O} - \Omega_i\|_{\text{fro}}^2\right) \quad (64)$$

where in our experiments we set $\sigma = 1/2$, $\Omega_1 = \text{diag}(1, 1, 1)$, $\Omega_2 = \text{diag}(-1, -1, 1)$, and $\Omega_3 = \text{diag}(-1, 1, -1)$. For dequantization we use rejection sampling to draw samples from the posterior. Then, with these fixed samples, we use batches of 100 samples to train the ambient and dequantization distributions.

Element	Notation	Description
Ambient Euclidean Space	$\mathcal{X} = \mathbb{R}^m$	Euclidean space in which the manifold of interest is embedded
Ambient Density	$\pi_{\mathcal{X}}(\cdot \theta)$	A flexible family of densities parameterized by $\theta \in \mathbb{R}^{n_{\text{amb}}}$ on \mathcal{X}
Change-of-Variables Mapping	$G : \mathcal{X} \rightarrow \mathcal{Y} \times \mathcal{Z}$	A smooth mapping satisfying the conditions of corollary 1 or theorem 1 where \mathcal{Z} is an auxiliary manifold.
Dequantization Density	$\tilde{\pi}_{\mathcal{Z}}(\cdot \phi, y)$	A non-vanishing family of dequantization distributions parameterized by $\phi \in \mathbb{R}^{n_{\text{deq}}}$ and possibly depending on $y \in \mathcal{Y}$.
Loss Function	$\mathcal{L} : \mathbb{R}^{n_{\text{amb}} \times n_{\text{deq}}} \rightarrow \mathbb{R}$	A loss function depending on $\{y_1, \dots, y_{n_{\text{obs}}}\}$, $\pi_{\mathcal{X}}$, and $\tilde{\pi}_{\mathcal{Z}}$ that is differentiable in θ and ϕ and captures the quality of the density estimate.

Table 5. The five elements that we use to dequantize a manifold into an ambient Euclidean space using a change-of-variables and dequantization density for marginalization.

F. Practical Considerations

F.1. The Ambient Euclidean Space

It is frequently the case that a manifold has a natural embedding into Euclidean space. For instance, the sphere \mathbb{S}^{m-1} is naturally embedded into \mathbb{R}^m . The Stiefel manifold is a subset of $\mathbb{R}^{n \times p}$ satisfying an orthonormality condition; therefore, it is naturally embedded into $\mathbb{R}^{n \times p}$. For some manifolds, the choice may require some consideration. For instance, a torus \mathbb{T}^2 may be regarded as a product manifold of two circles, each of which are naturally embedded into \mathbb{R}^2 so that the entire torus is embedded into \mathbb{R}^4 (this is called the *Clifford torus*). An alternative is the familiar embedding of the torus as a “doughnut” in \mathbb{R}^3 , although in this case it may be non-obvious how to construct a suitable mapping G between \mathbb{R}^3 , the doughnut torus, and some auxiliary choice of one-dimensional manifold.

F.2. The Mapping G and Auxiliary Manifold \mathcal{Z}

We have seen several examples wherein manifolds of interest appear alongside an auxiliary manifold when an ambient Euclidean space is transformed under a change-of-variables. In general, one would like to identify a transformation $G : \mathcal{X} \rightarrow \mathcal{Y} \times \mathcal{Z}$, satisfying the conditions of theorem 1 or corollary 1, such that it will be straightforward to formulate importance sampling random variables on \mathcal{Z} so as to obtain the marginal density on \mathcal{Y} .

F.3. Dequantization Density

Dequantization densities $\tilde{\pi}_{\mathcal{Z}}$ on \mathcal{Z} has to respect the constraints of the auxiliary manifold. For instance, if $\mathcal{Z} = \mathbb{R}_+$ we must choose a dequantization density whose support is the positive real numbers and which is non-vanishing. The requirement that $\tilde{\pi}_{\mathcal{Z}}$ be non-vanishing (that is, $\tilde{\pi}_{\mathcal{Z}}(z) > 0$ for all $z \in \mathcal{Z}$) is important so as to avoid division-by-zero singularities in the importance sampling formula eq. (15). We have already seen some examples of dequantization densities that respect the constraints of the auxiliary manifold in section 5. In each of these cases, the dequantization distribution is parameterized (for example, the Gamma distribution is parameterized by its shape and scale); it may be desirable to choose these parameters to depend on the location $y \in \mathcal{Y}$. To accomplish this, one may construct a neural network with parameters ϕ and input y whose output is the parameterization of the dequantization distribution. Thus the dequantization distribution may be in general expressed as $\tilde{\phi}_{\mathcal{Z}}(\cdot|\phi, y)$.

G. Evaluation Metrics

Given a density $\pi_{\mathcal{Y}}(y) \propto \exp(-u(y))$, known up to proportionality, we consider several performance metrics for the dequantization method we propose. The error of the first order moment is defined by,

$$\left\| \mathbb{E}_{y \sim \pi_{\mathcal{Y}}} [y] - \mathbb{E}_{\hat{y} \sim \hat{\pi}_{\mathcal{Y}}} [\hat{y}] \right\|_2. \quad (65)$$

The error of the second (centered) moment is defined by

$$\left\| \text{Cov}_{y \sim \pi_{\mathcal{Y}}} (y) - \text{Cov}_{\hat{y} \sim \hat{\pi}_{\mathcal{Y}}} (\hat{y}) \right\|_{\text{fro}}. \quad (66)$$

The Kullback-Leibler divergence of $\hat{\pi}_{\mathcal{Y}}$ and $\pi_{\mathcal{Y}}$ is

$$\text{KL}(\hat{\pi}_{\mathcal{Y}} \parallel \pi_{\mathcal{Y}}) \stackrel{\text{def.}}{=} \mathbb{E}_{\hat{y} \sim \hat{\pi}_{\mathcal{Y}}} \log \frac{\hat{\pi}_{\mathcal{Y}}(\hat{y})}{\pi_{\mathcal{Y}}(\hat{y})} \quad (67)$$

$$= \mathbb{E}_{\hat{y} \sim \hat{\pi}_{\mathcal{Y}}} [\log \hat{\pi}_{\mathcal{Y}}(\hat{y}) + u(\hat{y})] + \log Z, \quad (68)$$

where Z is the normalizing constant of $\pi_{\mathcal{Y}}(y)$. We can estimate Z via importance sampling according to

$$Z = \mathbb{E}_{\hat{y} \sim \hat{\pi}_{\mathcal{Y}}} \left[\frac{\exp(-u(\hat{y}))}{\hat{\pi}_{\mathcal{Y}}(\hat{y})} \right], \quad (69)$$

which permits us to compute a Monte Carlo estimate of the Kullback-Leibler divergence. The reverse direction of the KL-divergence $\text{KL}(\pi_{\mathcal{Y}} \parallel \hat{\pi}_{\mathcal{Y}})$ may be similarly computed.

Let $\{\hat{y}_1, \dots, \hat{y}_n\}$ be a collection of independent identically-distributed samples from $\hat{\pi}_{\mathcal{Y}}$. The number of effective independent samples is the quantity,

$$\text{ESS} \stackrel{\text{def.}}{=} \frac{\left(\sum_{i=1}^n \omega_i \right)^2}{\sum_{i=1}^n \omega_i^2} \quad (70)$$

where $\omega_i = \exp(-u(\hat{y}_i)) / \hat{\pi}_{\mathcal{Y}}(\hat{y}_i)$. See [Gower & Dijksterhuis \(2004\)](#); [Liu \(2008\)](#) for details on the ESS metric. Following [Rezende et al. \(2020\)](#), we report the relative ESS, which is the ratio of the effective sample size and n , the number of samples. When a Monte Carlo approximation of the evaluation metric is required, we use rejection sampling in order to obtain samples from the density $\pi_{\mathcal{Y}}$.

H. Proof of Theorem 1

Proposition 6. Let $A \subseteq \mathbb{R}^m$ and let $G : A \rightarrow \mathbb{R}^n$ be a smooth function. Suppose $m < n$. Define the embedded manifold $M \stackrel{\text{def.}}{=} G(A)$. Let π be a real-valued, continuous function on M . Then,

$$\int_M \pi(x) \, d\text{Vol}(x) = \int_A \pi(G(t)) \cdot \sqrt{\det((\nabla G(t))^\top (\nabla G(t)))} \, dt \quad (71)$$

where $d\text{Vol}$ is the volume measure on M .

Proof. See Jones (2004). □

Corollary 4. Define,

$$\pi_{\mathbb{R}^m}(t) \stackrel{\text{def.}}{=} \pi(G(t)) \cdot \sqrt{\det((\nabla G(t))^\top (\nabla G(t)))}. \quad (72)$$

Then rearranging immediately implies,

$$\pi(G(t)) = \frac{\pi_{\mathbb{R}^m}(t)}{\sqrt{\det((\nabla G(t))^\top (\nabla G(t)))}}, \quad (73)$$

which is the manifold change-of-variables formula.

What follows now is a more detailed exposition on this result using Riemannian geometry.

Let U be an open subset of \mathbb{R}^m . Let G be a continuous function from $U \rightarrow \mathbb{R}^n$ that is a homeomorphism on its image. That is, defining $\mathcal{M} \stackrel{\text{def.}}{=} \{G(x) : x \in \mathbb{R}^m\} \subset \mathbb{R}^n$, we find that G has a continuous inverse on \mathcal{M} . As a subset of \mathbb{R}^n , we can equip \mathcal{M} with the subspace topology and find that \mathcal{M} is topological m -manifold. Under these assumptions, it immediately follows that (\mathcal{M}, G^{-1}) is a *global* coordinate chart in the sense of differential geometry.

If we further assume that G and its inverse are smooth functions (in the sense of ordinary calculus), then it follows that \mathcal{M} is globally diffeomorphic to U . Evidently, our discussion allows $m \leq n$. If the Jacobian (in the sense of ordinary calculus) of G , denoted $\nabla G : U \rightarrow \mathbb{R}^{n \times m}$, has the property that at every $x \in U$, $\text{rank}(\nabla G(x)) = m$, then G is called a smooth immersion; this is equivalent to ∇G having full-rank at each $x \in U$. Moreover, because G is homeomorphic onto its image, G is also a smooth embedding.

The tangent space of a smooth manifold can be constructed as the vector space of velocities that a particle moving along the manifold may exhibit at a point. Formally, let $(a, b) \subset \mathbb{R}$ be an open interval and let $x : (a, b) \rightarrow U$ be a parameterized smooth curve in U . The composition $y \stackrel{\text{def.}}{=} G \circ x : (a, b) \rightarrow \mathcal{M}$ is then a parameterized smooth curve on \mathcal{M} . The velocity of y is then computed as,

$$\frac{d}{dt} y(t) = \frac{d}{dt} (G \circ x)(t) = \nabla G(x(t)) \dot{x}(t). \quad (74)$$

From the preceding discussion, $\nabla G(x(t)) \in \mathbb{R}^{n \times m}$ is a matrix of full-rank and therefore has m linearly-independent n -dimensional columns. Since $\dot{x}(t) \in \mathbb{R}^m$ can be arbitrary, we find that the tangent space of \mathcal{M} at $y(t)$ is the vector space spanned by the columns of $\nabla G(x(t))$; note that these basis vectors depend only on the position in U and not on time. Given $y \in \mathcal{M}$, we denote the tangent space by $T_y \mathcal{M} = \{\nabla G(x)c : c \in \mathbb{R}^m, x = G^{-1}(y)\}$ which is a vector subspace of \mathbb{R}^n . In the following, we make use of the common identification $T_x \mathbb{R}^m \cong \mathbb{R}^m$.

A smooth manifold can be turned into a Riemannian manifold by equipping its tangent spaces with an inner product called the Riemannian metric. Formally, given $y \in \mathcal{M}$, $g(y) \mapsto \langle \cdot, \cdot \rangle_y$ where $\langle \cdot, \cdot \rangle_y : T_y \mathcal{M} \times T_y \mathcal{M} \rightarrow \mathbb{R}$ is an inner product. Given the discussion so far, there is no prescription for a Riemannian metric. However, we may “prefer” the Riemannian metric that is induced from the ambient Euclidean space \mathbb{R}^n . For $\tilde{y} \in \mathbb{R}^n$, the Euclidean metric is defined by $\langle u, v \rangle_{\tilde{y}} = u^\top v$ where $u, v \in T_{\tilde{y}} \mathbb{R}^n \cong \mathbb{R}^m$. The induced metric on $\mathcal{M} \subset \mathbb{R}^n$ is then defined by $\langle u, v \rangle_y = u^\top v$ where u and v are viewed as vectors in \mathbb{R}^n satisfying $u, v \in T_y \mathcal{M}$.

Given a metric on \mathcal{M} , we can compute an associated metric on U called the *pullback metric*. The pullback metric is defined by,

$$\tilde{g}(x)(\tilde{u}, \tilde{v}) = g(G(x))(\nabla G(x)\tilde{u}, \nabla G(x)\tilde{v}) \quad (75)$$

$$= \tilde{u}^\top \nabla G(x)^\top \nabla G(x)\tilde{v} \quad (76)$$

where $\tilde{u}, \tilde{v} \in T_x \mathbb{R}^m \cong \mathbb{R}^m$. From the condition that $\nabla G(x)$ is a matrix of full-rank for each $x \in U$, it can be shown that $\nabla G(x)^\top \nabla G(x)$ is a positive definite matrix. Hence the pullback metric is a proper inner product. Unlike the induced metric on \mathcal{M} which has no real dependency on $y \in \mathcal{M}$, the pullback metric does depend on $x \in U$ through $\nabla G(x)^\top \nabla G(x)$. The pullback metric can be regarded as the expression of the induced metric on \mathcal{M} in the global coordinates of U . Indeed, if $y = G(x)$, recall that every $u \in T_y \mathcal{M}$ can be expressed as $u = \nabla G(x)\tilde{u}$ where $\tilde{u} \in \mathbb{R}^m$; the unique \tilde{u} can be computed from

$$\tilde{u} = (\nabla G(x)^\top \nabla G(x))^{-1} \nabla G(x)^\top u. \quad (77)$$

In our construction, we have described how to induce a metric on \mathcal{M} via the Euclidean metric in the embedding space. We then described how the metric materializes in the global coordinate system via the pullback metric. We are now in a position to state how these objects inform integration on Riemannian manifolds. We have the following theorem.

Theorem 2. Let $dVol$ denote the Riemannian volume element on \mathcal{M} when the metric on \mathcal{M} is the induced Euclidean metric from \mathbb{R}^n . Given a smooth function $f : \mathcal{M} \rightarrow \mathbb{R}$, its integral over \mathcal{M} can be expressed in terms of the global coordinate system as,

$$\int_{\mathcal{M}} f(y) dVol(y) = \int_U f(G(x)) \cdot \sqrt{\det(\nabla G(x)^\top \nabla G(x))} dx. \quad (78)$$

A proof of this result may be found in [Jones \(2004\)](#). More sophisticated variants of this result may be found textbooks on differential geometry; see, *inter alia*, [Lee \(2003\)](#).

If $\pi_{\mathcal{M}}$ is a density on \mathcal{M} , $y \sim \pi_{\mathcal{M}}$ and $A \subset \mathcal{M}$, then we have,

$$\Pr_{y \sim \pi_{\mathcal{M}}} [y \in A] = \int_{\mathcal{M}} \mathbf{1}\{y \in A\} \cdot \pi_{\mathcal{M}}(y) dVol(y) \quad (79)$$

$$= \int_U \pi_{\mathcal{M}}(G(x)) \cdot \mathbf{1}\{G(x) \in A\} \cdot \sqrt{\det(\nabla G(x)^\top \nabla G(x))} dx \quad (80)$$

$$= \Pr_{x \sim \pi_U} [x \in G^{-1}(A)] \quad (81)$$

where

$$\pi_U(x) = \pi_{\mathcal{M}}(G(x)) \cdot \sqrt{\det(\nabla G(x)^\top \nabla G(x))} \quad (82)$$

which, upon rearrangement, is the manifold change-of-variables formula.

Given a subset $A \subset \mathcal{M}$, we define its volume by,

$$\int_A dVol(y) = \int_{G^{-1}(A)} \sqrt{\det(\nabla G(x)^\top \nabla G(x))} dx. \quad (83)$$

Such a definition of volume is sometimes called the “surface measure” and it is a generalization of arclength in the one-dimensional setting. Moreover, this notion of volume coincides with the m -dimensional Hausdorff area of A ; this is a consequence of the *area formula* and a detailed discussion can be found in [Federer \(1969\)](#).

I. Embedded Manifolds

A smooth manifold \mathcal{X} of dimension k is a second-countable Hausdorff space such that for every $x \in \mathcal{X}$ there is a homeomorphism between a neighborhood of x and \mathbb{R}^k . By the Whitney Embedding Theorem (see, *inter alia*, Lee (2003)), every smooth manifold can be smoothly embedded into Euclidean space of dimension $2k$. It is frequently possible to express an embedded manifold as the zero level-set of a constraint function: Let $g : \mathbb{R}^m \rightarrow \mathbb{R}^k$ be a smooth function and define $\mathcal{X} \stackrel{\text{def.}}{=} \{x \in \mathbb{R}^m : g(x) = 0\}$. If $\nabla g(x) \in \mathbb{R}^{k \times m}$ is a matrix of full-rank for every $x \in \mathcal{X}$, we say that \mathcal{X} is an embedded manifold of rank k . To see how these definitions apply, let us consider some examples.

I.1. Hypersphere

The sphere in \mathbb{R}^3 is the zero level-set of the constraint function $g(x) \stackrel{\text{def.}}{=} x^\top x - 1$.

I.2. Torus

The torus is the preimage of the constraint function $g : \mathbb{R}^4 \rightarrow \mathbb{R}^2$ defined by

$$g(x) \stackrel{\text{def.}}{=} \begin{pmatrix} x_1^2 + x_2^2 - 1 \\ x_3^2 + x_4^2 - 1 \end{pmatrix}. \quad (84)$$

I.3. Stiefel Manifold

A constraint function for the Stiefel(n, p) manifold is $g : \mathbb{R}^{n \times p} \rightarrow \mathbb{R}^{n \times n}$ defined by $g(\mathbf{M}) = \mathbf{M}^\top \mathbf{M} - \text{Id}_n$. Using the $\text{vec} : \mathbb{R}^{m \times n} \rightarrow \mathbb{R}^{mn}$ isomorphism, Stiefel(n, p) may also be embedded into \mathbb{R}^{np} .